PCCP

Accepted Manuscript

ROYAL SOCIETY OF CHEMISTRY

www.rsc.org/pccp

Solvent impact on the singlet and triplet states of selected fluorine corroles – absorption, fluorescence, and optoacoustic studies

Bartosz Bursa[1], Danuta Wróbel[1*], Bolesław Barszcz[1,2], Michał Kotkowiak[1], Olena Vakuliuk[3], Daniel T. Gryko[3*], Łukasz Kolanowski[4], Marek Baraniak[4], Grzegorz Lota[4]

[1]Faculty of Technical Physics, Institute of Physics, Poznan University of Technology, Piotrowo 3, 60-965 Poznan, Poland

[2]Institute of Molecular Physics, Polish Academy of Sciences, Smoluchowskiego 17, 60-179 Poznan, Poland

[3]Institute of Organic Chemistry, Polish Academy of Sciences, Kasprzaka 44/52, 01-224 Warsaw, Poland

[4]Institute of Chemistry and Technical Electrochemistry, Poznan University of Technology, Berdychowo 4, 60-965 Poznan, Poland

Corresponding authors:

prof. D. Wróbel; e-mail: danuta.wrobel@put.poznan.pl

prof. D. T. Gryko; e-mail: dtgryko@icho.edu.pl

Abstract

This paper examines the influence of aprotic solvents on spectroscopic properties as well as the energy deactivation of two free-base corrole dyes substituted with C_6F_5 and/or 4-$NO_2C_6H_4$ groups. Absorption, fluorescence and laser-induced optoacoustic spectroscopy have been used to follow the singlet and triplet states of fluorine corroles belonging to the A_2B and A_3 type in toluene (TL), chloroform (CL), dimethylformamide (DMF), dimethyl sulfoxide (DMSO) and also in solvent mixtures. Changes in the absorption and fluorescence spectra are influenced by the type of solvent mixture. The fluorescence behaviors of the two investigated corroles were extremely different – fluorescence of the nitro-corrole in TL is dramatically quenched in the presence of DMF. In contrast, fluorescence quenching of the fluorine corrole in DMF-TL mixtures is substantially weakened. Absorption, fluorescence, triplet population as well as singlet oxygen generation parameters are evaluated. The spectral experimental data are supported by quantum chemical calculations - time-dependent density functional theory (TD-DFT) and cyclic voltammetry experiments. The presented results are discussed from a view point of aggregation, tautomerization, and deprotonation effects occurring in the corroles.

Keywords: tautomerization, protonation/deprotonation, fluorescence quantum yield/life-time, triplet population, single oxygen

Abbreviations: toluene – TL, chloroform – CL, dimethylformamide – DMF, dimethyl sulfoxide – DMSO, ferrocene – FC, laser induced optoacoustic spectroscopy – LIOAS, time-dependent density functional theory – TD-DFT, chlorophyll – Chl, pheophytin – Pheo, internal conversion – IC, intersystem crossing – ISC, highest occupied molecular orbital – HOMO, lowest unoccupied molecular orbital – LUMO

1. Introduction

Because of their unique properties and abundancy, porphyrins have been the most commonly used systems in modeling light-energy harvesting and conversion over the past decades.[1] Efforts to improve photophysical properties of porphyrins have encouraged the use of other porphyrinoids such as corroles, a unique family of dyes. Although corroles were first reported several decades ago by Johnson and Kay,[2] they have not been thoroughly investigated due to synthetic challenges . Recent advances in synthetic procedures have improved and advanced corrole chemistry,[3,4] and thus provide a venue for new possible applications.

Corroles are aromatic macrocycles that are analogues of porphyrins dyes, but with one less carbon.[2] They are characterized by the reduced C_{2V} symmetry with regard to the D_{2h} and D_{4h} symmetry of porphyrins due to the absence of one *meso* carbon bridge (direct pyrrole-pyrrole linkage). Consequently, corroles' photophysical characteristics are different that of porphyrins including: stronger absorption in the red region of the spectrum, greater fluorescence quantum yield, larger Stokes shift, different reactivity and profound differences in coordination chemistry.[2,5–7]

A variety of corroles consisting of different molecular structure and in different solvents[8–14] and in solid matrices[15–18] have been investigated through physical/photophysical and chemical/photochemical experiments to examine their singlet/triplet behavior,[8,19] tautomerization, protonation[11,13,20,21] and interactions with fullerene as an electron acceptor.[18,22–24]

Although the photophysical properties of corroles have been investigated, further studies are needed to make these compounds applicable. In earlier work, our laboratory conducted basic spectral investigations of selected substituted *meso*-corroles and their dyads with fullerene.[21,23,25] In these studies, we discovered that corroles are very good electron donating species when covalently linked to fullerene and provided evidence for their molecular orientation when arranged in solid substrates.[23,25] The influence of solvent polarity on spectral properties of corroles and the locations of exchangeable protons have been the subjects of a few studies.[5,21,26] However, the question of the protonation and deprotonation effects has not yet been fully resolved although some studies on tautomers of *meso*-pentafluorophenyl-substituted corroles in chloroform have been previously studied.[21]

In the present study, we focused our attention on the properties of A_3-corrole possessing three C_6F_5 substituents at *meso*-positions and *trans*-A_2B-corrole bearing one 4-$NO_2C_6H_4$ group at position 10. These studies include an investigation of protonation/deprotonation with the use of polar and non-polar solvents and their mixtures. We also provide UV-vis spectra. Moreover, laser-induced optoacoustic spectroscopy (LIOAS) was used for the first time to determine the population of the triplet states, singlet oxygen generation and triplet thermal deactivation. The experimental data are supported by computational calculations via time-dependent density functional theory (TD-DFT) to obtain information on the distribution of electron density in the systems.

Computational calculations as well as electrochemical measurements are very important in determining the molecular energy levels of dyes, when embedded in an organic solar cell. The highest occupied molecular orbital (HOMO) and the lowest unoccupied molecular orbital (LUMO) can be determined by means of cyclic voltammetry.[27]

2. Materials and methods

2.1. UV-vis absorption and fluorescence

In these studies we present investigations of two free-based corrole dyes (10-(4-nitrophenyl)-5,15-bis(pentafluorophenyl)corrole (**1**) and 5,10,15-tris(pentafluorophenyl)corrole (**2**). The detailed description of chemical synthesis of the dyes was described previously.[28,29] The molecular structures of the dyes under investigations are shown in Fig. 1.

Spectroscopic grade toluene (TL), chloroform (CL), dimethylformamide (DMF) and dimethyl sulfoxide (DMSO) were purchased from POCH Poland S.A. Ground state

absorption spectra were monitored with a UV-Vis Varian Cary 4000 spectrophotometer in an ES quartz cuvette over the range of 350-700 nm; all measurements were done at room temperature. Fluorescence was measured using a Hitachi F-4500 fluorimeter (λ_{exc} = 405 nm). Fluorescence lifetime was obtained with a 1.5 ns pulse, 405 nm LED excitation source . Fluorescence responses were collected over the range of 430-900 nm (excitation and emission spectra).

The fluorescence quantum yields (Φ_F) were determined using the classical formula:

$$\Phi_F = \Phi_{Ref} \frac{F_s}{F_r} \frac{(1-10^{-A_r})}{(1-10^{-A_S})} \frac{n_s^2}{n_r^2} \quad (1)$$

where A is the absorbance at the excitation wavelength, F is the area under the fluorescence and *n* is the refraction index. The subscripts *r* and *s* refer to the reference and to the sample of unknown quantum yield, respectively. For reference, chlorophyll *a* in methanol was used (Φ_{ref} = 0.32).[30] The samples and as well as the reference were excited at the same wavelengths, 405 and 614 nm. Fluorescence lifetimes were estimated by fitting the decay data using a deconvolution procedure based on the EasyLife V software.

2.2. Quantum chemical calculations

To improve the interpretation of the experimental UV-Vis spectra we performed calculations of the transition energies via time-dependent density functional theory (TD-DFT). The chemical calculations were performed using the B3LYP hybrid functional (Becke 3-parameter exchange functional combined with Lee-Yang-Parr correlation functional) and the standard 6-31G basis set. Time dependent DFT calculations were performed using the equilibrium geometries of the molecules obtained from optimization for the investigated corroles (DFT, B3LYP/6-31G). Influence of solvent (CL, TL and DMSO) was taken into account using the Polarized Continuum Model (PCM) as implemented in the Gaussian 03 program package.[31] The first 200 optical transitions were calculated. To convolute the resulting transition energies and oscillator strengths into the absorption spectra, the GaussSum program was used.[32] The spectra were generated assuming FWHM (Full Width at Half Maximum) parameters at 3000 cm^{-1} for all transitions.

2.3. Electrochemical measurements

Cyclic voltammetry experiments were performed using a three-electrode cell: glassy carbon as a working electrode, platinum wire as a counter electrode, and Ag/AgCl as a reference electrode. The working electrode was polished with a suspension of Al_2O_3 in water

and rinsed in water and acetone on ultrasounds before experiments. Electrochemical measurements were carried out in a solution containing 10^{-5} M of examined corroles in methyl alcohol and toluene (ratio 1:1) as supporting electrolytes. The electrolyte was purged by nitrogen over 30 minutes before the test. The potential varied between -3 and 3 V vs. Ag/AgCl with a scan rate of 20 mV s^{-1}. All electrochemical measurements were performed with the use of the potentiostat/galvanostat VSP (BioLogic, France) equipped with a low current module.

The experiments were performed without and with illumination by a xenon 150W lamp.

2.4. LIOAS studies

To obtain additional information on the influence of corrole photophysical properties and the nature of the solvent on photothermal parameters, time-resolved photothermal signals were recorded using the LIOAS method. Specific details of LIOAS apparatus have been described by other groups.[26,33,34] For LIOAS experiments, corrole dyes are dissolved in CL, TL, DMF, and DMSO respectively. Ferrocene (FC), purchased from Sigma-Aldrich, and Ni-substituted pheophytin *a*[35] were chosen as calorimetric references due to their suitable spectral properties for LIOAS experiments. All measurements were carried out at ambient temperature, in air and argon atmosphere. The excitation wavelengths were 405 nm or 614 nm; the absorbance of the corrole was equal to 0.1 at the excitation wavelength.

The analysis of the LIOAS waveform was carried out according to the methods of Marti *et al.*[36] In this approach, the first maximum (H_{max}) of the LIOAS signal is expressed as:

$$H_{max} = k\alpha^{air}E_{hv}(1 - 10^{-A}), \quad (2)$$

where k is a proportionality factor that regards geometry and electric impedance of a device, α^{air} is a part of the energy changed into heat in an air atmosphere (in time shorter than a time resolution of the apparatus), A is absorbance of a sample and E_{hv} is the molar energy of incident photons (295.3 kJ·mol^{-1} at 405 nm and 194.8 kJ·mol^{-1} at 614 nm).

Part of the excitation energy exchanged into heat promptly (α parameter) and was calculated by direct comparison of the slopes in the linear region of the plots obtained for the corrole and for the reference dye in argon and air.[37]

The quantum efficiency of the triplet state population (Φ_T) could be evaluated with the use of the following equation:

$$E_T\Phi_T = E_{las}(1 - \alpha^{Ar}) - E_S\Phi_{Fl} \quad (3)$$

where α^{Ar} is the fraction of excitation energy exchanged into heat promptly in argon

atmosphere (in time shorter than a time resolution of the apparatus), E_S is energy of the singlet state in [kJ·mol^{-1}], E_T is energy of the triplet state and Φ_F is the quantum yield of fluorescence (Table 1). However, we do not know the exact value of E_T for the examined samples, therefore the Φ_T parameter can be only estimated based on $E_T\Phi_T$.

The efficiency of singlet oxygen generation (Φ_Δ) can be evaluated from the following equation:

$$\Phi_\Delta = \frac{E_{h\nu}}{E_\Delta}\left(1 - \alpha^{air}\right) - \frac{E_S}{E_\Delta}\Phi_F, \quad (4)$$

where α^{air} is the fraction of excitation energy exchanged into heat promptly in argon atmosphere (in time shorter than a time resolution of the apparatus), $E_{h\nu}$ is the molar energy of the incident photons and E_Δ is the energy of the oxygen singlet state (E_Δ = 94 kJ·mol^{-1}).

3. Results and discussion

3.1. Electronic absorption experiments in solvents and their mixtures

Both studied corroles showed good solubility in many organic solvents, particularly in TL, CL, DMF, and DMSO. The molecular structures and ground state electronic absorption spectra of (10-(4-nitrophenyl)-5,15-bis(pentafluorophenyl)corrole (**1**) and 5,10,15-tris(pentafluorophenyl)corrole (**2**) in TL, DMF and DMSO (concentration 10^{-4} – 10^{-6} M) are shown in Figs. 1-2, respectively.

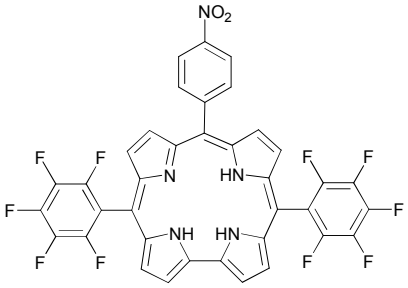

1

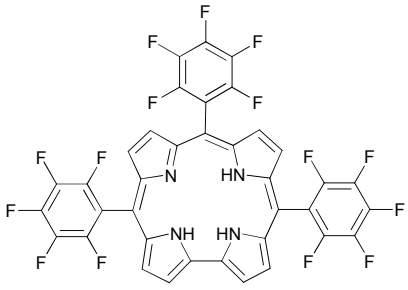

2

Fig. 1 Molecular structures of investigated corroles.

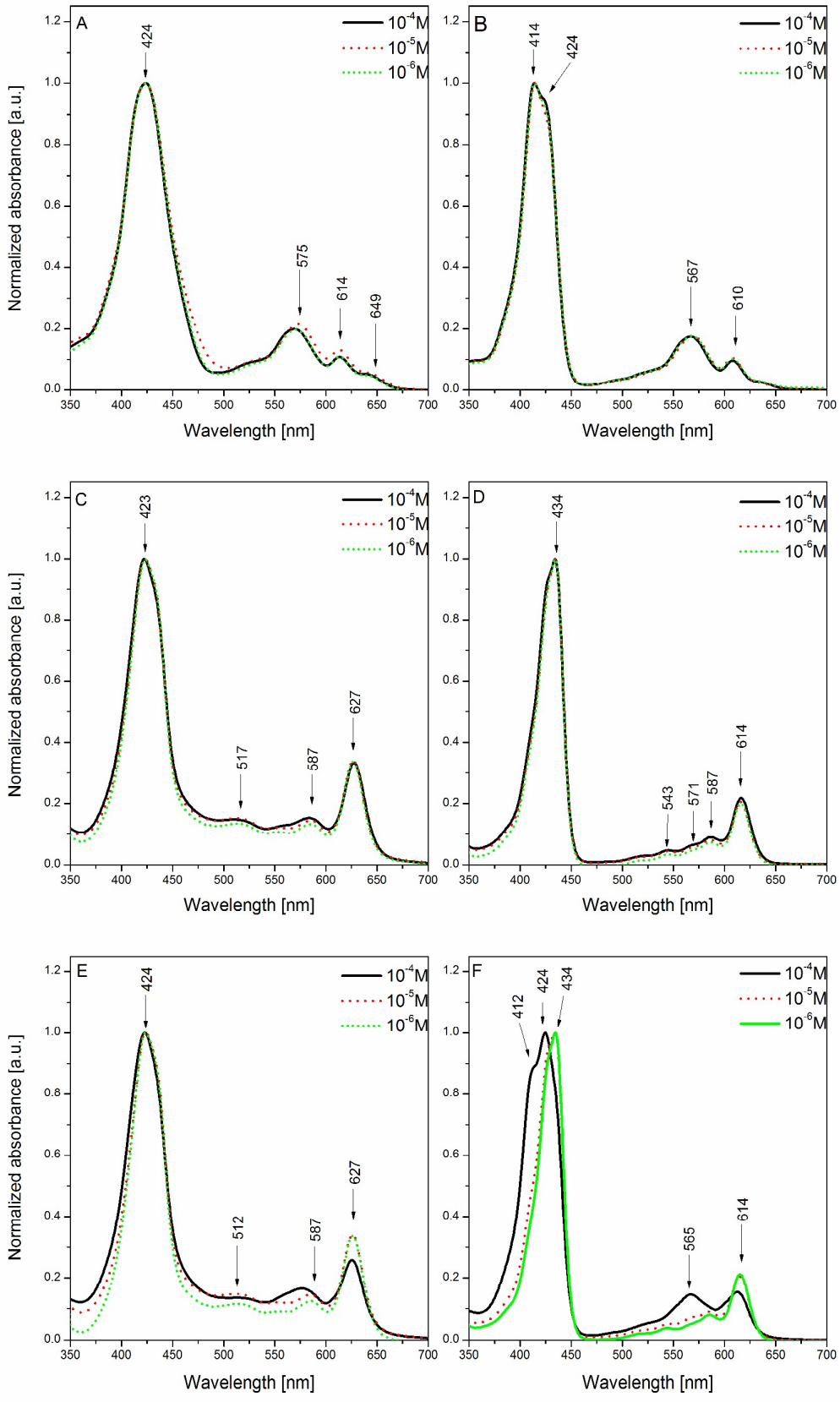

Fig. 2 Absorption spectra of corroles **1** (panels at left) and **2** (panels at right) in TL (A, B), DMF (C, D) and DMSO (E, F); concentration range 10^{-4} – 10^{-6} M. The absorption spectra were normalized to unity at the highest Soret band (424 nm).

The concentration of the sample had a marked effect on the absorption spectra for corrole **2** in DMSO as indicated by a blue shift in the wavelength maximum and the appearance of a shoulder peak at higher concentrations of **2** (Fig. 2, panel F); no such remarkable effects were observed in the spectra of **2** in TL and DMF (Fig. 2, panels B and D) Even though corroles are closely related to porphyrins, their absorption spectra have distinct differences: their absorption spectra are dominated by the π-π^* transitions with an intense and broad Soret band and a much lower intensity Q band.

We previously reported the assignment of the π-π^* electron transition in the Soret and Q bands of these corroles dissolved in CL.[21] The presence of the tautomeric T1 and T2 forms of the investigated corroles was clearly evident in the Soret regions as a broad band (sample **1**; Fig. 2, A) at 424 nm and more or less split bands (samples **1** and **2**; Fig. 2, B-F) with the maxima at 414–434 nm, depending on the dye. Some changes were also observed in the Q region of the spectra. No particular changes in the absorption spectra were observed for the samples at different concentrations thus showing the dominance of the tautomers' monomeric forms up to 10^{-4} M (except for **2** – Fig. 2 F). Solvent properties often cause π-π^* dyes to associate into dimers (J and H dimers)[38] or higher aggregated forms which show smaller or larger wavelength shifts. The best example of the dimer formation is chlorophyll (Chl)[30] which is a metallic coordinated porphyrin-like pigment. Chlorophyll dimers can be formed *via* direct or indirect interaction between magnesium of one Chl and an electron donating group of another molecule. However, in our studies, we used non-metallic free-based corroles without metal ions in the main molecular core, pheophytin (Pheo). Pheo is also able to make dimers and its dimerization can occur *via* π-π^* interaction at adequately high concentration. Thus, on the basis of behavior of the natural pigments and of other synthetic porphyrin-like molecules,[39–41] one can suppose the presence of poorly defined molecular aggregates; further, this phenomenon cannot be excluded in highly concentrated samples.

DMSO had a great influence on absorption with sample **2**. The DMSO was the most polar solvent (ε = 46.70) that was tested (DMF (ε = 37), CL (ε = 4.80) and TL (ε = 2.38)). Highly concentrated solution of corrole **2** in polar DMF did not show notable changes when compared to the same corrole dissolved in DMSO. However, it is worth noting that most

molecular aggregates are not created in polar solvents since polar solvents protect molecules against aggregate formation due to solvation.

Formations of aggregated forms of corroles address the phenomena of tautomerization, protonation/deprotonation, and distortion of the pyrrole ring. Solvent effects are evident in our absorption studies (Fig. 2 A – E as compared to Fig. 2F). The shape of the absorption bands differ mainly in the Soret region of **1** and **2** and the Q region of **2**. This observation can be attributed to differences in the molecular structure of **1** versus **2**, e.g., the presence of the nitro substituent group (in **1** – A_2B type tautomer) and pentafluorophenyl substituent (in **2** – A_3 type tautomer).

The tautomers T1 and T2 are difficult to distinguish in **1** (in TL – in Fig. 2A) because of their very similar energies. Otherwise, the bands in the Soret peak are clearly visible in the highly concentrated sample **2** in DMSO (Fig. 2F) – the bands with the maxima at 412 and 424 nm (10^{-4} M) are well separated (*versus* the Soret bands in the remaining spectra). This observation could originate from two sources: (i) a change in the relative amounts of T2 and T1, giving rise to varied band intensities at 412, 424, 434 nm, and (ii) the process of deprotonation, resulting in the short wavelength shift of the Soret band of different energy.[9,13,21] In an earlier report,[20] a deprotonation effect was observed in polar DMSO.

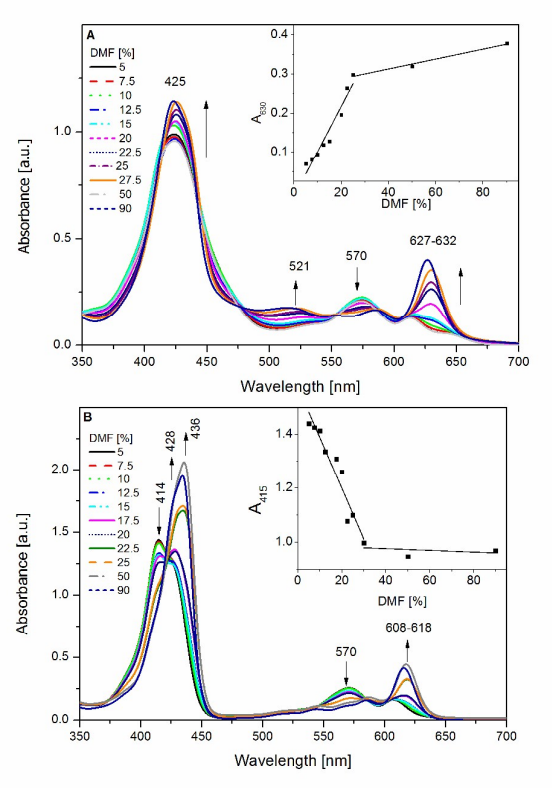

Fig. 3 Absorption spectra of corroles **1** (A) and **2** (B) in DMF and TL mixtures; concentration 10^{-5} M. Titration curve for corrole **1** (insert) and corrole **2** (insert).

We also recorded the absorption spectra of the corroles in mixtures of polar (DMF) and non-polar (TL) solvents (Fig. 3). These studies further confirmed a strong effect of solvents on dye behavior. Differences in the shapes and intensities were obvious in the Soret regions and in the Q bands of **1** and **2**. The most dramatic changes were observed in the Q region of **1** and **2** and also of **2** in the Soret region. The differences in the absorption spectra in the presence of different solvent ratios could be related to the dyes' molecular structures since the substituents in **1** and **2** are structurally unlike (nitrophenyl and pentafluorophenyl groups). Moreover, the asymmetry in the pyrrole-rings could result in replacing of the -NH groups around the main π-core ring, leading to changes in the equilibrium of tautomers T1 and T2;[9] in 100% TL *versus* 100% DMF, the changes in T1 and T2 were evident from the shift of the Soret band towards the longer wavelength, from 414 to 436 nm for **2.** Such an observation is characteristic for a deprotonated corrole.[14] The existence of the deprotonated form of the corrole **2** is further confirmed by the appearance of a species with higher intensity at longer wavelength; the 0-0 transition with the maximum at 620 nm. In the case of **1**, a bathochromic shift was not observed in the Soret region.

Titration curves (inserts in Fig. 3) showed two stages in the reactive kinetics. The changes in the absorbance value are about 85% in the sample **1** (Q band region) and about 93% in the sample **2** (Soret region). The distinct changes in band shapes that occurred after the addition of DMF to TL indicated the very strong polar influence of DMF on processes occurring in the dyes. TL is non-polar solvent, while DMF is polar-aprotic solvent and their dipole moments are quite different (0.36 D of TL *versus* 3.82 D of DMF). Consequently, the interaction between the corrole and TL is different compared to the dye and DMF. The changes in the spectra of the corroles could indicate the formation of aggregates however our previous absorption results and literature data[21] excludes this possibility. Although tautomerization could contribute to alternation of the spectra, our earlier papers[9,10] indicated that tautomerism is a rather weak phenomenon. One of the arguments supporting the slight influence of tautomerization[9,10,21] is the similar energy of both tautomers. A third possibility, from Ding *et al*.,[9] suggested that hydrogen bonding with the -NH group could cause changes in the structure of the molecules that are solvent-dependent. Similar effects were observed in porphyrins in apolar solvents.[42,43] The hydrogen linkage between NH and a solvent molecule was also observed in corroles[44] producing changes in the photophysical properties. Resonance effects related to the electron-withdrawing or electron-donating properties of substituents should also be considered. The changes in absorption spectra in polar solvent (DMF, DMSO) can also be discussed in terms of a mesomeric effect as shown for a phthalocyanine substituted with fluorine groups.[45]

Based on our experiments in the TL-DMF mixtures and the results presented in other papers,[9,10] we believe that deprotonation is the key influence on the absorption behavior of the samples **1** and **2** in the presence of the aprotic solvent DMF.

3.2. Fluorescence studies

We acquired the excitation and emission spectra of the corrole **2** (10^{-5} and 10^{-6} M) in DMSO (Fig. 4A–B). Using DMSO as a reference solvent allowed us to measure the effect of solvents with high polarity and to avoid (or to minimize) molecular aggregate formation. Only the corrole **2** in DMSO showed strong fluorescence with maxima at 621–625 and 674 nm (Fig. 4). Similar behavior had also been observed for other corroles.[8,20,46,47] The dominant fluorescence peak was assigned to emission of the tautomer T1; the much less intense shorter wavelength humps can have their origin in fluorescence of T2.[48,49] The fluorescence excitation spectra, when observed at 700 nm, were consistent with the UV-vis absorption spectra. The details of the fluorescence character of the corroles in non-polar chloroform have

been discussed in our previous paper[21] thus we will present the fluorescence spectra in the TL-DMF mixtures (of different DMF contribution (%) as shown in (Figs. 5 and 6.)

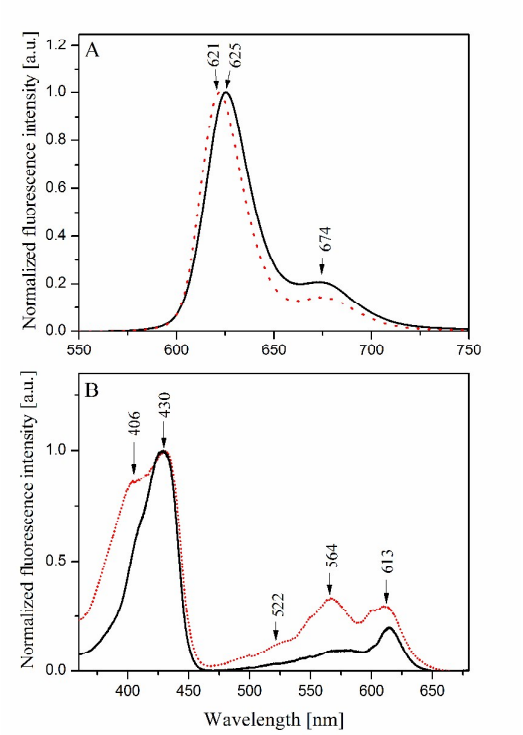

Fig. 4 Fluorescence spectra of corroles **2** and their excitation emission spectra in DMSO normalized at the maximal bands; A, λ_{exc} = 405 nm, B - λ_{obs} = 700 nm. Concentration 10^{-5} M (dotted red) and 10^{-6} M (straight black) were used. The spectra are normalized with respect to the most intense peak.

The fluorescence spectra of **1** and **2** (shown in Figs 4 and 5) differed markedly in their intensity, peak shapes, and location of the maxima. It is well known that the presence of nitro groups typically quenches the fluorescence of organic compounds to the level below the detection limit.[50] Accordingly we observed that fluorescence quantum yield of corrole **1** is much weaker than that of corrole **2** in TL (Table 1). The Φ_F value is larger (0.1) compared to the vast majority of known organic dyes of the same family. Furthermore, significant quenching of the fluorescence signal (~ 750-fold) was observed for corrole **1** after the addition of DMF to TL. The more DMF that was added, the stronger quenching was observed, the rate of fluorescence quenching at 658 nm is presented in Fig. 5B. Furthermore, the fluorescence bands shifted to shorter wavelengths (from 659 to 624 nm). In corroles and other porphyrin-like dyes, the macrocyclic π-electrons are involved in the fluorescence process. The lack of (or minimal) fluorescence of the sample **1** in the presence of DMF can be

attributed to the relocation of the majority of the electron density cloud from the macroring and from the nitro group – nitro substituents have a strong electron withdrawing character as seen in Fig. 8. This behavior can only be explained by considering molecule **1** as conjugated donor-acceptor (D-A) system with 4-$NO_2C_6H_4$ group acting as an electron acceptor and the corrole core acting as an electron donor. Although the dihedral angle between the corrole core and benzene ring at position 10 is large (possibly ~68°)[44] it can still provide means for strong interaction of both moieties. The decrease of fluorescence quantum yield while moving towards polar solvents is a well-known phenomenon for polarized D-A compounds.[50]

Corrole **2** is substituted with C_6F_5 groups exclusively and behaves differently. Moreover, the Stokes shifts of the bands with respect to the transitions at 659 nm (sample **1**) and at 628-645 nm (sample **2**) were about 20-30 nm, indicating strong deprotonation, mostly observed for the T2 tautomer. The changes in the fluorescence band locations in the TL-DMF mixture can be clearly seen in insert Fig.5, an enlargement of the fluorescence spectra. Band maxima of the fluorescence in TL-DMF for dye **1** occur at 659 and 624 nm for low concentration of DMF (to 30%); the emission maxima or a hump appear in the spectra of **1** and are assigned to T1 and T2 emission, respectively. In solvent ratios of 50/50, 90/10 and 100/0, an emission peak at 639 nm originated from the T2 tautomer (the band at 658 nm is actually not seen).[11,21]

In contrast, the influence of TL-DMF solvent on the sample **2** fluorescence was opposite quenching by DMF was not observed. The band shapes and main bands shifting (from 645 to 624 nm – (0/100)) were nearly unchanged upon the addition of more DMF to the solvent mixture. However, the band shifts towards the higher energy part of the spectrum indicating deprotonation of the corroles. Nevertheless, upon addition of DMF, a large increase in fluorescence was observed (Fig. 6), supporting a very strong effect of DMF on tautomer T2 fluorescence.

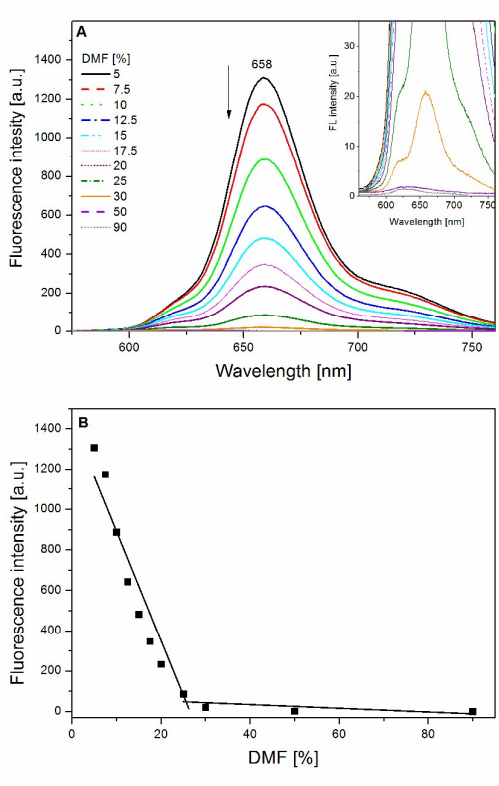

Fig. 5 Fluorescence (A - λ_{exc} = 405 nm) in DMF-TL mixture, the same spectra in the enlarged scale (insert); and titration curve (B).

The lack of notable changes in the band shapes upon addition of DMF to TL was a strong indicator of the negligible influence of DMF on processes occurring in the corrole dyes. Similar fluorescence behavior has been observed by Kruk *et al.*[20,46] for other NH meso-dichloropyrimidinyl corrole tautomers. In their work, the T2 tautomer emission was also intense. Fluorescence studies also confirmed the deprotonation process, as exhibited in sample **2** (the fluorine corrole) in DMSO.

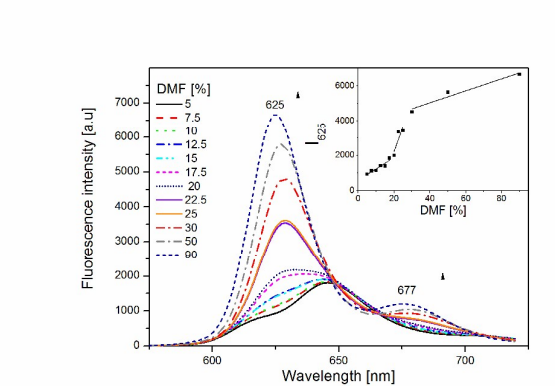

Fig. 6 Fluorescence (λ_{exc} = 405 nm) spectra of corrole **2** in DMF-TL mixture. Titration curve for corrole **2** (insert).

The fluorescence kinetics curves for **2** in different solvents are shown in Fig. 7. The evaluated life-time values (Table 1) ranged from 5.12 – 6.21 ns (depending on the dye) and are characteristic of porphyrin-like dyes. They confirm the monomeric corrole emission in corroles **1** and **2** in TL and DMF. The deconvolution procedure used in our evaluation gave the typical mono-exponential fluorescence decay curves in TL and DMF in the range of 10^{-4} – 10^{-6} M. However, we were not able to recognize the life times of tautomers T1 and T2. The values of fluorescence quantum yields (Table 1) were markedly different when one compares the results of the samples **1** and **2** in TL (0.07-0.10) *versus* those in polar DMF (0.32-0.34) and in DMSO (0.47). In **1,** strong fluorescence quenching was evident (in both DMF and DMSO) – the Φ_F and τ values dropped dramatically, almost to zero (see Table 1). The bi-exponential decay observed for sample **2** in DMSO may indicate the presence of two tautomers emitting with different lifetimes.

Table 1 The optical parameters, absorption and fluorescence parameters of corroles **1** and **2** in selected solvents; FWHM – full width at half maximum (calculated with the Gaussian component program) Φ_F – fluorescence quantum yield, τ – fluorescence life time.
ε- dielectric constant, D - dipole moment [Debye], Fb – free base corrole

Solvent	ε	D	Dye	Soret FWHM [cm^{-1}]	Major contribution	$\Phi_{F(405)}$	$\Phi_{F(614)}$	τ [ns]
TL	2.38	0.36	**1**	2903 (conc. 10^{-4}-10^{-6} M)	Fb /mesomeric effect	0.10	0.08	6.15±0.04
			2	2126 (conc. 10^{-4}-10^{-6} M)	Fb	0.10	0.08	6.21±0.02

DMF	37	3.8	**1**	2230 (conc. 10^{-4}-10^{-6} M)	mesomeric effect/ deprotonated	<0.01	<0.01	-
			2	1523 (conc. 10^{-4}-10^{-6} M)	deprotonated	0.36	0.36	5.12±0.06
DMSO	46.7	3.9	**1**	2465 (conc. 10^{-4} M)	mesomeric effect / deprotonated	<0.01	-	-
				2219 (conc. 10^{-5}-10^{-6} M)				
			2	2323 (conc. 10^{-4}M)	deprotonated	0.48	-	5.33±0.28 (4.45%)
				1363 (conc. 10^{-5}-10^{-6} M)				0.37±0.07 (95.55%)

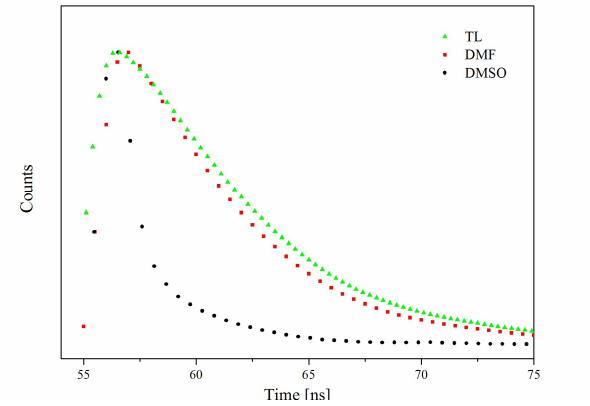

Fig. 7 Fluorescence kinetics of **2** in TL, DMF and DMSO (concentration 10^{-5} M); λ_{exc} = 405 nm.

3.3. Quantum chemical calculations

To improve the interpretation of the experimental UV-vis spectra, we calculated the transition energies via TD-DFT. We then compared the absorption and fluorescence spectra with the TD-DFT results and the HOMO/LUMO states. In our previous paper[21] we presented the TD-DFT results of the isolated corroles **1** and **2**. Here, we have extended TD-DFT calculations for these corroles in TL, CL and DMSO.

Table 2 illustrates the solvent influence on the calculated energy levels of the frontier molecular orbitals of the corroles **1** and **2**. Increasing relative permittivity of the solvent increased the energy levels. In **2**, both HOMO and LUMO energy increased with the increase in solvent permittivity. Consequently, the energy gap between the HOMO and the LUMO remained constant (2.53 eV). Corrole **1** showed a slightly different behavior. The HOMO level increased, LUMO level did not change much thus decreasing the HOMO-LUMO energy gap in **1** from 2.45 eV (for isolated corrole) to 2.12 eV (for solution in DMSO). This outcome suggested that corrole **1** is susceptible to solvent effects. The reduction of the energy gap

caused by the solvent was also observed by Panda *et al.*[51] for the A_2B_2 type porphyrin derivatives. However, these investigators reported that the direction of the changes in the HOMO and LUMO energy levels were opposite (decrease of the orbital energy in solvent). The influence of the solvent on the energy levels of **1** appeared not only in energy values but also in localization of the molecular orbital. For the isolated **1**, the HOMO was localized on the corrole ring while the LUMO was on the corrole ring and partially on the nitro substituent.[21] For **1** in solution (in all the considered solvents), the localization of the HOMO were similar and the LUMO was localized on the nitrophenyl (in DMSO - Fig. 8A) and on both the nitrophenyl substituent and partially on the corrole ring in TL (Fig. 8C). Compound **2** did not exhibit such behavior, indicating that the position of the orbital is solvent-independent (Fig. 8B,D).

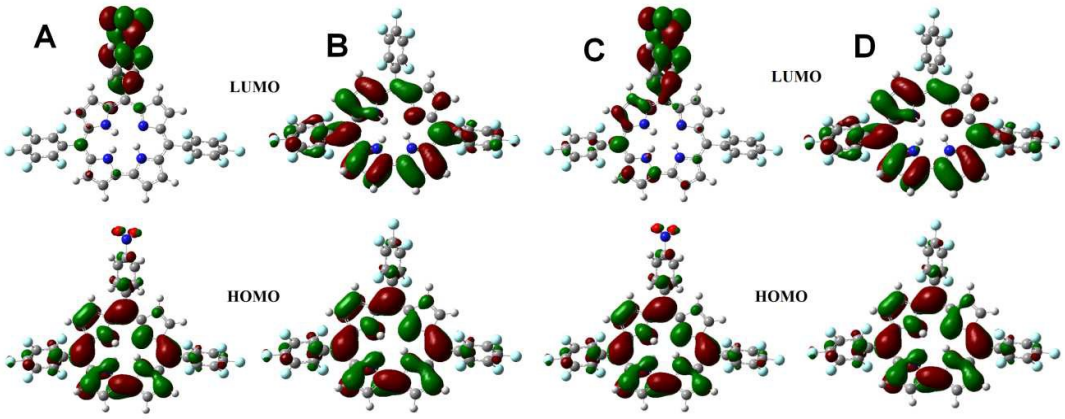

Fig. 8 The contour plots of the TD-DFT calculated frontier molecular orbitals of the corrole **1** (A,C) and **2** (B,D); A, B in DMSO; C, D in TL. (T2 tautomer).

The π-electrons in the corrole macrorings are responsible for fluorescence. Taking into account the HOMO-LUMO results presented in Fig. 8, it is evident that a high density of electrons are localized on the 4-$NO_2C_6H_4$ substituent and very slightly on the core ring in the corrole **1**. The weak fluorescence of sample **1** may be caused by relocation of the majority of the electron density cloud from the macroring to the nitrophenyl group upon excitation in the LUMO level. This is not the case for **2**, which is substituted with the fluorine groups.

The question now arrives as to the fluorescence of **1** in TL. There were a few examples presented in papers[52,53] showing fluorescence quenching of dyes due to the electron withdrawing character of the nitro group introduced to the maternal dye. On the other hand, it was evidently shown how much the fluorescence of dyes with the nitro group is affected by

the molecular dye structure, solvent, the type of substituent linked to dye molecules and location of a substituent. Many authors have shown quenched fluorescence in dyes containing nitro-groups.[50] There are some evidences presenting how the location of the nitro-substituent can influence dye emission behavior.[52–55] The nitro group is one of the most electrophilic moieties and has an electron deficiency. This group is known as a substituent with the negative mesomeric effect, relatively to the sp^3 carbon. However, one has also to take into account the asymmetry in the location of the NH group in the macrocycle. The presence of the three NH groups leads to the asymmetry of the electron density distribution on the pyrrole rings what is evidenced by our TD-DFT results of **1** in TL and shown in Fig. 8C - a high density of electrons is predominantly localized in the nitro group and also partially in the core ring in the sample **1** in the LUMO state. Moreover, one cannot exclude an influence of the two C_6F_5 being near the core π-electrons thus changing the electron density in the corrole 1. Therefore, we have come to the conclusion that the weak fluorescence of sample **1** originates from the π-electron redistribution in the corrole macroring resulting from the NH asymmetry in the presence of the fluorine-groups.

Table 2 The TD-DFT calculated values of the molecule dipole moment (in Debye units) and the HOMO and LUMO energies (in eV) of investigated corroles.

Solvent	Corrole **1**				Corrole **2**			
	Dipole moment	HOMO	LUMO	Δ_{H-L}	Dipole moment	HOMO	LUMO	Δ_{H-L}
none	6.3172	- 5.58	- 3.13	2.45	3.7685	- 5.63	- 3.10	2.53
toluene	7.4079	- 5.39	- 3.07	2.31	4.5052	- 5.47	- 2.94	2.53
Fchlorofor m	8.0358	- 5.31	- 3.07	2.23	4.9068	- 5.39	- 2.83	2.56
DMSO	8.7525	- 5.22	- 3.10	2.12	5.3455	- 5.31	- 2.78	2.53

The TD-DFT calculated spectra (Fig. 9) of the investigated corroles showed that in the presence of solvents, theoretical calculations showed increased intensity and a red shift in the absorption bands. This result is quite similar to those obtained by Panda et al.[51] for porphyrins, where the bands in the calculated solution spectra were also increased and red-shifted in comparison to the gas phase result. A closer look at the transitions involved in computation of the absorption bands revealed that the Soret band in the isolated **2** consisted of three main transitions below 400 nm. The solution spectra show that two bands increased significantly and moved above 400 nm (Fig. 9, right). Similar behavior was observed for the Q band region and the differences between the corrole-solution spectra in TL, CL and DMSO

were relatively small. The corrole **1** showed stronger effects - the Soret band behavior was similar to that of **2** (increasing, red-shifted transitions), but the Q band region was different. For the isolated **1** the Q band consisted of four transitions. These transitions not only increased and red-shifted in the corrole-solution spectra, but their shifts and intensities were solvent-dependent. The energetically lowest transitions in the corrole-solvent spectra were observed at 626, 657, and 691 nm for the corroles in TL, CL, and DMSO respectively. Appropriate transitions in the corrole-solution spectra for **2** showed a very small blue shift with increased solvent permittivity (553, 552, 551 nm for TL, CL and DMSO respectively). Major contributions of the calculated transitions are collected in Table S1 (for **1**) and Table S2 (for **2**). We observed completely different behavior for corroles **1** *versus* **2**. For the corrole **2**, the dominant contribution (36%) in the mentioned first transition was H-1→LUMO while the rest of the transition involves other orbitals including the HOMO→LUMO transition (25%). This situation changes when we consider the presence of solvent – the contribution of the HOMO→LUMO transition became dominant and increased up to 50% for **2** in DMSO. The corrole **1** also showed a complex composition of the first transition for the isolated molecule – the dominant contribution was HOMO→L+1 (53%) while the contribution of HOMO→LUMO was similar to that for **2** (22%). However, the influence of the solvent caused the first transition in **1** in the presence of solvents to be almost the pure HOMO→LUMO (89-94%) and the remaining contributions were much less significant. As a consequence, the calculated solution spectra of **1** showed more differences in comparison to the spectra of the isolated species, as compared to corrole **2**. The detailed data of the theoretical calculations are gathered in Tables S1 and S2.

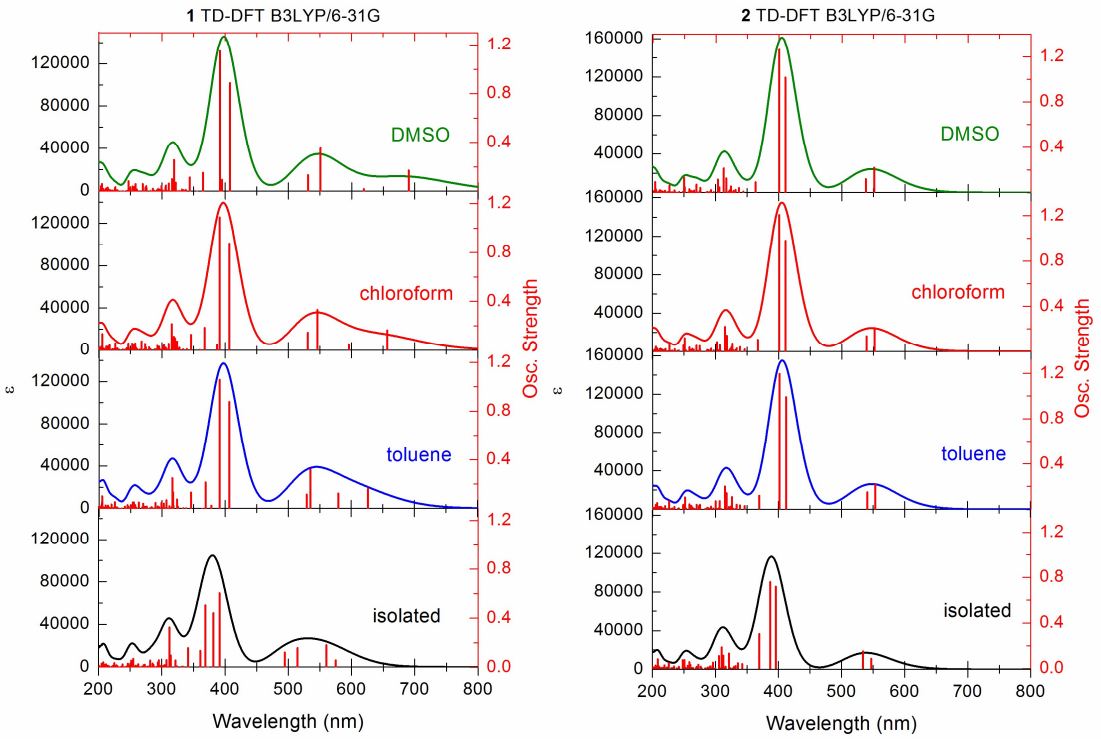

Fig. 9 The TD-DFT calculated electronic transitions (oscillator strengths *versus* wavelength) of the corroles **1** (left side) and **2** (right side) together with the convoluted UV-vis spectra.

3.4 Electrochemical experiments

Cyclic voltammetry is an electrochemical method that provides information on the oxidation and reduction processes of the compounds. It can be also used for estimation of HOMO and LUMO. The oxidation process is associated with removal of an electron from the HOMO level, on the other hand, the reduction process corresponds to an electron being located on the LUMO level. This means that, the HOMO/LUMO can be determined on the value of first oxidation and on the value of the first reduction electrochemical potentials. The mathematic equation according to the HOMO/LUMO energy level and electrochemical potential (for Ag/AgCl reference electrode):

$$E_{HOMO/LUMO} = -(E_{OX/RED} + 4.4)eV \quad (5)$$

E_{OX} and E_{RED} are the onset potentials of oxidation and reduction, respectively. The onset potentials of oxidation and reduction were specified from tangents being intersected between the peak and the baseline.[56–60]

Fig. 10 shows the results of cyclic voltammetry measurements. The onset potentials of oxidation of the corroles were observed at about 1.1 - 1.2 V, while the reduction potentials

were -0.8 and -1.0 V for the corroles **1** and **2**, respectively. Based on equation (5), the HOMO/LUMO energy levels were calculated and summarized in the Table 3. It can be concluded, that the corrole **1** is characterized by lower LUMO energy value. It means that corrole **2** is better electron acceptor than corrole **1**.[58] The TD-DFT calculated values of the HOMO and LUMO levels (Table 2) are in quite good agreement with the values obtained from the electrochemical studies. All the energy levels are slightly overestimated and the difference is bigger for the LUMO levels. However, the relation between the results obtained for corrole **1** and **2** from both methods (TD-DFT and cyclic voltammetry) is preserved. It can be seen in the mutual positions of HOMO and LUMO levels in both corroles, and in the size of the HOMO-LUMO energy gap (smaller for corrole **1**).

It is worth mentioning that during illumination, the energy gap increases in the case of the corroles **1** and **2**. However, a clearer enlargement of the energy gap after illumination by a xenon lamp was observed for the corrole **2**. Under lighting an electron can be excited from the HOMO to LUMO level only if the ionization potential difference between the donor and the acceptor affinity is larger than the binding energy of the exciton (electron-electron hole system). Moreover, under illumination the HOMO energy level decreases, but LUMO energy level increases. Therefore, the energy gap increases after lighting.[27]

The functionalization of corroles strongly influences on the properties of the macrocycle, therefore detailed analysis is essential due to practical point of view. From cyclic voltammetry measurements, it can be seen that the reduction potential equal's -0.8 V and -1.0 V for corrole **1** and corrole **2**, respectively. It can be stated that $–NO_2$ groups are electron-withdrawing species which provide the reduction processes to more positively value of potential. Corrole rings because of high electron density can operate as donor, on the other hand $–NO_2$ substituents can act as acceptor, resulting in lower energy of LUMO level.[61–63]

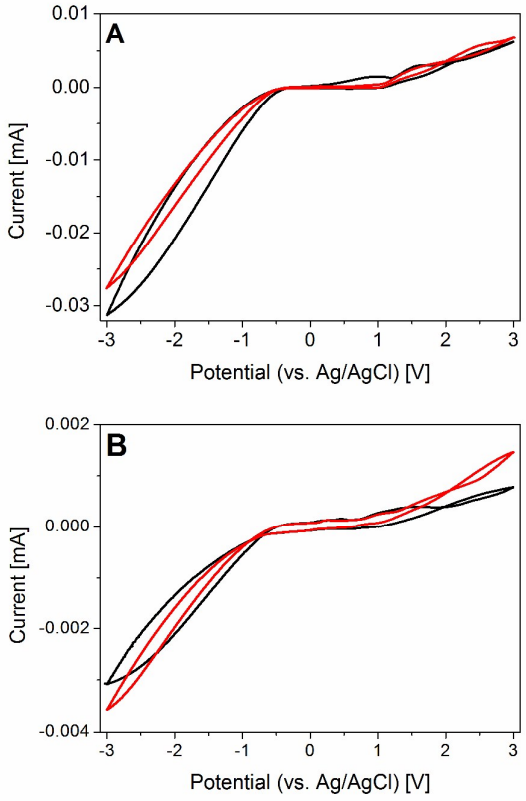

Fig. 10 Cyclic voltammetry of corrole **1** (A) and corrole **2** (B) in TL, in the dark (black lines) and under illumination (red lines).

Table 3 The potentials of oxidation and reduction and HOMO and LUMO energies (in eV) of the tested corroles calculated from cyclic voltammetry measurements

Sample	E_{ox} [V]	E_{red}[V]	HOMO [eV]	LUMO [eV]	Δ_{H-L} [eV]
TL 1	1.1	-0.8	-5.50	-3.6	1.90
TL 1 light	1.1	-0.9	-5.60	-3.5	2.10
TL 2	1.1	-1.0	-5.50	-3.4	2.10
TL 2 light	1.25	-1.2	-5.65	-3.2	2.45

3.5. Laser induced optoacoustic spectroscopy (LIOAS) experiments – triplet state studies

The activation and deactivation of the triplet state of corroles **1** and **2** were investigated by LIOAS experiments. LIOAS was used for the first time to evaluate the triplet state population and determine the Φ_Δ in corroles **1** and **2**. Fig. 11 illustrates the relation between the H_{max} of the sample **1** and **2** in TL and DMF as a function of the energy (E_{hv}) applied by a 405 nm laser.

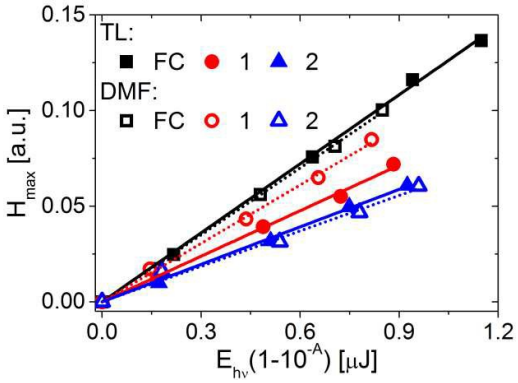

Fig. 11 LIOAS signal H_{max} of the sample **1** (red), **2** (blue) and ferrocene (black) in TL (closed symbols) and in DMF (opened symbols) as a function of the laser energy E_{hv}; λ_{exc} = 405 nm; $R^2 \geq 0.99$.

The LIOAS results of the corroles **1** and **2** in TL, CL, DMF and DMSO are collected in Table 4. α^{air} and α^{Ar} present the part of energy exchanged to heat promptly in the time shorter than time resolution of the used device. The α^{air} and α^{Ar} values for the samples **1** and **2** were dependent on the solvents used in the experiments. The α^{air} values were about 0.66–0.86 (sample **1**) and 0.53–0.61 (sample **2**) in TL, CL, DMF and DMSO when excited at 405 nm. When excitation was at 614 nm, their values were lower, ranging from 0.41–0.61. The variations in the α^{air} can originate from the different contributions of the tautomers T2 and T1 in energy deactivation. The 405 nm laser beam excites mostly the tautomer T2, resulting in T2 participation in thermal deactivation. In contrast, when the 614 nm light was used in the experiment, the tautomer T1 was mostly excited and it contributed to light energy conversion. The yield of the triplet population, expressed as the $E_T\Phi_T$ values, was also dependent on the type of solvent used: they ranged from 51 to 86 kJ·mol^{-1} for the sample **1** and 60 – 124 kJ·mol^{-1} for the sample **2** in all used solvents.

An evaluation of the LIOAS data in the context of the fluorescence results can provide insights into the thermal deactivation processes in which the singlet and triplet states of the corroles are involved. The observed intensity of corroles emission competes with the

processes of the internal conversion S_1-S_0 (IC). The emission of corroles in the present study was affected by DMF and DMSO – sample **1** fluorescence was strongly quenched while that of sample **2** was **not.** Moreover, α^{Ar} is higher for the sample **2** in comparison to the sample **1**, thus, we cannot suppose higher intersystem crossing quantum yields in **1** i.e. population of the triplet state.

The Φ_Δ were also evaluated (Table 4). The process that is responsible for singlet oxygen formation is the interaction between the excited triplet and oxygen. The Φ_Δ was in the range of 0.41 to almost 1.00, depending on the solvent. These results indicate the efficient generation of singlet oxygen by the corroles studied in this paper. Similar values (0.51-0.77) were determined by Ventura *et al*. by investigations of free-based corroles in TL by singlet oxygen luminescence experiments.[8]

Table 4 LIOAS parameters for the sample **1** and **2** in solvents. $E_T\Phi_T$ and Φ_Δ are calculated based on equations (3) and (4)

Solvent	α^{Ar} (±0.05)		$E_T\Phi_T$ [kJ·mol^{-1}] (±6 kJ·mol^{-1})		α^{air} (±0.05) excited at 405nm/614 nm		Φ_Δ (±0.05) excited at 405nm/614 nm	
	1	**2**	**1**	**2**	**1**	**2**	**1**	**2**
DMSO	0.77	0.48	65	60	0.86	0.56	0.41	0.41
DMF	0.82	0.47	51	88	0.86/0.60	0.53/0.41	0.41/0.81	0.75/0.49
CL	0.76	0.55	64	115	0.85	0.61	0.42	1.03
TL	0.65	0.52	86	124	0.66/0.52	0.61/0.50	0.86/0.84	1.02/0.88

4. Conclusions

We have investigated the relationship between the strength of electron-withdrawing substituents and their photophysical properties as well as the deprotonation of free base corroles in non-polar and polar solvents. The replacement of moderately electron-withdrawing C_6F_5 group with strongly electron-withdrawing 4-$NO_2C_6H_4$ substituent led to significant changes of optical properties due to the formation of strong donor-acceptor system. The changes in absorption spectra indicated that in the presence of polar solvents (DMF, DMSO), a mesomeric form of corrole possessing NO_2 group and deprotonated forms of both corroles are present. Our hypothesis concerning different ratios of various tautomers for these two corroles is supported for the NO_2-corrole by fluorescence quenching. We also demonstrated that an increase of DMF in DMF/TL mixture leads to a hypsochromic shift of the wavelength of the fluorescence emission maximum of the tris(pentafluorophenyl)corrole (TPFC), which confirms the formation of the H_2AB^- form.[14]

The TD-DFT calculations explain the different behaviour of the samples' NO_2-corrole and TPFC in solution. They show that the changes in the UV-vis spectra of the NO_2-corrole in solutions are related to localization of the LUMO on the nitro group which is quite distinct from that of TPFC. Our results also show that energies of the frontier orbitals of both corroles are sensitive to the solvent permittivity while the HOMO-LUMO gap is influenced by the solvent only in the case of NO_2-corrole.

The onset potentials of oxidation of the corroles were observed at about 1.1 - 1.2 V, while the reduction potentials were -0.8 and -1.0 V for the corroles **1** and **2**, respectively. The HOMO and LUMO results evaluated with the TD-DFT are consistent with cyclic voltammetry measurements.

Tautomerization and deprotonation of the samples is very important because of their influence on the behavior of NO_2-corrole and TPFC in non-polar and/or polar solvents. The changes in the absorption band shapes confirm the effect of simple manipulation of the protonation/deprotonation states with properly selected polarity of solvents. It is worth noting that only some tautomers were obtained by the simple manipulation of solvent polarity. This result reflects the asymmetry of the tetrapyrrole ring; such that the two tautomeric forms are distinct and are structurally quite different.[64] The laser induced optoacoustics studies show high quantum efficiency of the triplet state population and high singlet oxygen generation both of samples NO_2-corrole and TPFC. Moreover, for the aprotic solvents DMSO and DMF, similar photophysical parameters were observed.

On the basis of our experimental and chemical calculations, the optical properties of corroles open the pathway for their applications such as construction of polarity-probes and in dye-sensitized solar cells.

Acknowledgments

This work was supported by Poznan University of Technology (grant No. 06/62/DSPB/0216, BB, DW, MK) and Polish National Centre for Research and Development (grant OLAE+). We thank Eli M. Espinoza (UC Riverside) for amending the manuscript.

References

1 D. Holten, D. F. Bocian and J. S. Lindsey, *Acc. Chem. Res.*, 2002, **35**, 57–69.
2 A. W. Johnson and I. T. Kay, *J. Chem. Soc.*, 1965, 1620–1629.
3 Z. Gross, N. Galili and I. Saltsman, *Angew. Chem. Int. Ed. Engl.*, 1999, **38**, 1427–1429.
4 F. DSouza, R. Chitta, K. Ohkubo and S. Fukuzumi, *J. Am. Chem. Soc.*, 2008, **130**, 14263–14272.

5 R. Voloshchuk, D. T. Gryko, M. Chotkowski, A. I. Ciuciu and L. Flamigni, *Chem. - A Eur. J.*, 2012, **18**, 14845–14859.
6 B. Koszarna and D. T. Gryko, *J. Org. Chem.*, 2006, **71**, 3707–3717.
7 D. T. Gryko and K. E. Piechota, *J. Porphyr. Phthalocyan.*, 2002, **6**, 81–97.
8 B. Ventura, A. Degli Esposti, B. Koszarna, D. T. Gryko and L. Flamigni, *New J. Chem.*, 2005, **29**, 1559–1566.
9 T. Ding, E. A. Alemán, D. A. Modarelli and C. J. Ziegler, *J. Phys. Chem. A*, 2005, **109**, 7411–7417.
10 J. F. B. Barata, M. G. P. M. S. Neves, A. C. Tomé, M. A. F. Faustino, A. M. S. Silva and J. A. S. Cavaleiro, *Tetrahedron Lett.*, 2010, **51**, 1537–1540.
11 W. Beenken, M. Presselt, T. H. Ngo, W. Dehaen, W. Maes and M. Kruk, *J. Phys. Chem. A*, 2014, **118**, 862–871.
12 A. L. Ward, H. L. Buckley, W. W. Lukens and J. Arnold, *J. Am. Chem. Soc.*, 2013, **135**, 13965–13971.
13 Y. B. Ivanova, V. A. Savva, N. Z. Mamardashvili, A. S. Starukhin, T. H. Ngo, W. Dehaen, W. Maes and M. M. Kruk, *J. Phys. Chem. A*, 2012, **116**, 10683–10694.
14 M. Kruk, T. H. Ngo, V. Savva, A. Starukhin, W. Dehaen and W. Maes, *J. Phys. Chem. A*, 2012, **116**, 10704–10711.
15 C. L. He, F. L. Ren, X. B. Zhang and Z. X. Han, *Talanta*, 2006, **70**, 364–369.
16 S. Yamauchi, M. Tanabe, Y. Ohba, K. Sugisaki, K. Toyota, K. Sato, T. Takui and I. Saltsman, *Chem. Phys. Lett.*, 2012, **521**, 64–68.
17 L. Tortora, G. Pomarico, S. Nardis, E. Martinelli, A. Catini, A. D'Amico, C. Di Natale and R. Paolesse, *Sensors Actuators, B Chem.*, 2013, **187**, 72–77.
18 C. Chen, Y. Z. Zhu, Q. J. Fan, H. Bin Song and J. Y. Zheng, *Tetrahedron Lett.*, 2013, **54**, 4143–4147.
19 J. H. Palmer, A. C. Durrell, Z. Gross, J. R. Winkler and H. B. Gray, *J. Am. Chem. Soc.*, 2010, **132**, 9230–9231.
20 M. Kruk, T. H. Ngo, V. Savva, A. Starukhin, W. Dehaen and W. Maes, *J. Phys. Chem. A*, 2012, **116**, 10704–11.
21 B. Bursa, B. Barszcz, W. Bednarski, J. P. Lewtak, D. Koszelewski, O. Vakuliuk, D. T. Gryko and D. Wróbel, *Phys. Chem. Chem. Phys.*, 2015, **17**, 7411–23.
22 K. Lewandowska, B. Barszcz, J. Wolak, A. Graja, M. Grzybowski and D. T. Gryko, *Dyes Pigments*, 2013, **96**, 249–255.
23 B. Bursa, D. Wrobel, K. Lewandowska, A. Graja, M. Grzybowski and D. T. Gryko, *Synth. Met.*, 2013, **176**, 18–25.
24 A. Graja, *Mol. Cryst. Liq. Cryst.*, 2012, **554**, 31–42.
25 K. Lewandowska, B. Barszcz, A. Graja, B. Bursa, A. Biadasz, D. Wróbel, W. Bednarski, S. Waplak, M. Grzybowski and D. T. Gryko, *Synth. Met.*, 2013, **166**, 70–76.
26 S. E. Braslavsky and G. E. Heibel, *Chem. Rev.*, 1992, **92**, 1381–1410.
27 A. Shafiee, M. M. Salleh and M. Yahaya, *Sains Malays*, 2011, **40**, 173–176.
28 D. T. Gryko and B. Koszarna, *Synthesis (Stuttg).*, 2004, **2004**, 2205–2209.
29 D. T. Gryko and B. Koszarna, *Org. Biomol. Chem.*, 2003, **1**, 350–357.
30 H. Scheer, *Chlorophylls*, CRC Press, Boca Raton Ann Arbor Boston London, 1991.
31 Gaussian 03, Revision D.01, M. J. Frisch, G. W. Trucks, H. B. Schlegel, G. E. Scuseria, M. A. Robb, J. R. Cheeseman, J. A. Montgomery, T. Vreven, K. N. Kudin, J. C. Burant, J. M. Millam, S. S. Yengar, J. Tomasi, V. Barone, B. Mennucci, M. Cossi, G. Scalmani, N. Rega, G. A. Petersson, H. Nakatsuji, M. Hada, M. Ehara, K. Toyota, R. Fukuda, J. Hasegawa, M. Ishida, T. Nakajima, Y. Honda, O. Kitao, H. Nakai, M. Klene, X. Li, J. E. Knox, H. P. Hratchian, J. B. Cross, V. Bakken, C. Adamo, J. Jaramillo, R. Gomperts, R. E. Stratmann, O. Yazyev, A. J. Austin, R. Cammi, C.

Pomelli, J. W. Ochterski, P. Y. Ayala, K. Morokuma, G. A. Voth, P. Salvador, J. J. Dannenberg, V. G. Zakrzewski, S. Dapprich, A. D. Daniels, M. C. Strain, O. Farkas, D. K. Malick, A. D. Rabuck, K. Raghavachari, J. B. Foresman, J. V Ortiz, Q. Cui, A. G. Baboul, S. Clifford, J. Cioslowski, B. B. Stefanov, G. Liu, A. Liashenko, P. Piskorz, I. Komaromi, R. L. Martin, D. J. Fox, T. Keith, M. A. Al-Laham, C. Y. Peng, A. Nanayakkara, M. Challacombe, P. M. W. Gill, B. Johnson, W. Chen, M. W. Wong, C. Gonzalez and J. A. Pople, *Gaussian, Inc., Wallingford CT*, 2004.

32 N. M. O'Boyle, A. L. Tenderholt and K. M. Langner, *J. Comput. Chem.*, 2008, **29**, 839–845.

33 D. Wróbel, A. Biadasz and B. Bursa, *Int. J. Thermophys.*, 2012, **33**, 716–732.

34 Rosencwaig A, *Photoacoustics and Photoacoustic Spectroscopy*, Wiley, New York, 1980.

35 M. Pilch, A. Dudkowiak, B. Jurzyk, J. Łukasiewicz, A. Susz, G. Stochel and L. Fiedor, *Biochim. Biophys. Acta - Bioenerg.*, 2013, **1827**, 30–37.

36 C. Martí, O. Jürgens, O. Cuenca, M. Casals and S. Nonell, *J. Photochem. Photobiol. A Chem.*, 1996, **97**, 11–18.

37 M. Kotkowiak, J. Łukasiewicz and A. Dudkowiak, *Int. J. Thermophys.*, 2013, **34**, 588–596.

38 Michael Kasha, *Radiat. Res.*, 1963, **20**, 55–70.

39 F. Tantussi, F. Fuso, M. Allegrini, N. Micali, I. G. Occhiuto and L. Mons, *Nanoscale*, 2014, **6**, 10874–10878.

40 T. Zhuang, S. Sasaki, T. Ikeuchi, J. Kido and X.-F. Wang, *RSC Adv.*, 2015, **5**, 45755–45759.

41 T. Doane, A. Chomas, S. Srinivasan and C. Burda, *Chem. - A Eur. J.*, 2014, **20**, 8030–8039.

42 J. R. Weinkauf, S. W. Cooper, A. Schweiger and C. C. Wamser, *J. Phys. Chem. A*, 2003, **107**, 3486–3496.

43 P. Bhyrappa and P. Bhavana, *Chem. Phys. Lett.*, 2001, **342**, 39–44.

44 D. Ding, J. D. Harvey and C. J. Ziegler, *J. Porphyr. Phthalocyan.*, 2005, **9**, 22–27.

45 A. Siejak, D. Wróbel and R. M. Ion, *J. Photochem. Photobiol. A Chem.*, 2006, **181**, 180–187.

46 Y. B. Ivanova, V. A. Savva, N. Z. Mamardashvili, A. S. Starukhin, T. H. Ngo, W. Dehaen, W. Maes and M. M. Kruk, *J. Phys. Chem. A*, 2012, **116**, 10683–10694.

47 M. Kruk, T. H. Ngo, P. Verstappen, A. Starukhin, J. Hofkens, W. Dehaen and W. Maes, *J. Phys. Chem. A*, 2012, **116**, 10695–10703.

48 A. Ghosh, T. Wondimagegn and A. B. J. Parusel, *J. Am. Chem. Soc.*, 2000, **122**, 5100–5104.

49 R. S. Becker, *Theory and Interpretation of Fluorescence and Phosphorescence*, New York, Wiley Inte., 1969.

50 B. Valeur, *Molecular Fluorescence Principles and Applications*, Wiley-VCH Verlag, 2002.

51 M. K. Panda, G. D. Sharma, K. R. Justin Thomas and A. G. Coutsolelos, *J. Mater. Chem.*, 2012, **22**, 8092–8102.

52 S. Hachiya, K. Asai and G. Konishi, *Tetrahedron Lett.*, 2013, **54**, 1839–1841.

53 T. Ueno, Y. Urano, H. Kojima and T. Nagano, *J. Am. Chem. Soc.*, 2006, **128**, 10640–10641.

54 A. Bolduc, Y. Dong, A. Guérin and W. G. Skene, *Phys. Chem. Chem. Phys.*, 2012, **14**, 6946–6956.

55 B. Carlotti, F. Elisei, U. Mazzucato and A. Spalletti, *Phys. Chem. Chem. Phys.*, 2015, **17**, 14740–14749.

56 B. W. D'Andrade, S. Datta, S. R. Forrest, P. Djurovich, E. Polikarpov and M. E. Thompson, *Org. Electron.*, 2005, **6**, 11–20.

57 P. I. Djurovich, E. I. Mayo, S. R. Forrest and M. E. Thompson, *Org. Electron.*, 2009, **10**, 515–520.

58 A. Misra, P. Kumar, R. Srivastava, S. K. Dhawan, M. N. Kamalasanan and S. Chandra, *Indian J. Pure Appl. Phys.*, 2005, **43**, 921–925.

59 C. Ye, M. Li, J. Luo, L. Chen, Z. Tang, J. Pei, L. Jiang, Y. Song and D. Zhu, *J. Mater. Chem.*, 2012, **22**, 4299–4305.

60 P. Petrova, P. Ivanov, Y. Marcheva, R. Tomova, *Bulg. Chem. Commun.*, 2013, **45**, 159–164.

61 M. Stefanelli, G. Pomarico, L. Tortora, S. Nardis, F. R. Fronczek, G. T. McCandless, K. M. Smith, M. Manowong, Y. Fang, P. Chen, K. M. Kadish, A. Rosa, G. Ricciardi and R. Paolesse, *Inorg. Chem.*, 2012, **51**, 6928–6942.

62 S. Nardis, M. Stefanelli, P. Mohite, G. Pomarico, L. Tortora, M. Manowong, P. Chen, K. M. Kadish, F. R. Fronczek, G. T. McCandless, K. M. Smith and R. Paolesse, *Inorg. Chem.*, 2012, **51**, 3910–3920.

63 M. Stefanelli, F. Mandoj, M. Mastroianni, S. Nardis, P. Mohite, F. R. Fronczek, K. M. Smith, K. M. Kadish, X. Xiao, Z. Ou, P. Chen and R. Paolesse, *Inorg. Chem.*, 2011, **50**, 8281–8292.

64 S. Szymański, P. Paluch, D. T. Gryko, A. Nowak-Król, W. Bocian, J. Sitkowski, B. Koszarna and J. Śniechowska, *Chem. Eur. J.*, 2014, **20**, 1720–1730.